

Scaling Cloud Attenuation Statistics with Link Elevation in Earth-space Applications

Lorenzo Luini and Carlo Capsoni

Abstract—A methodology to scale cloud attenuation statistics with link elevation in Earth-space applications is presented in this contribution. The vertical and horizontal distribution of clouds is investigated by taking advantage of the liquid water content observed by the Cloud Profiling Radar onboard the CloudSat Earth Observation satellite. Besides casting some light on the actual validity of the customary assumption of horizontal uniformity for clouds, analytical expressions for the scaling factor are proposed to derive cloud attenuation statistics on slant paths from attenuation predictions at zenith. The proposed methodology could be beneficial to improve the accuracy of the model currently adopted by the ITU-R in recommendation P.840-6, especially when low elevation links (e.g. between 5° and 20°) are involved.

Index Terms— Electromagnetic propagation, cloud effects, satellite communications.

I. INTRODUCTION

EARTH-space communication systems are nowadays quickly increasing in number and complexity to accommodate, on one side, the growing demand of advanced multimedia and interactive services (e.g. Internet via satellite) and, on the other side, the download of huge amount of data collected by high-resolution instruments onboard Earth Observation satellites. These needs are pushing towards the employment of higher carrier frequencies (e.g. Ka, Q and V bands), which offer larger bandwidths and limited congestion and interference issues. On the other side, above 20 GHz the detrimental impact of the atmosphere on electromagnetic waves increases considerably, not only due to hydrometeors, which always play the most relevant role [1],[2], but also owing to suspended liquid water, which becomes more and more significant, especially for links at low elevation θ , both in terms of specific attenuation and because of the high occurrence probability of clouds (typically between 40% and 80% of the yearly time at mid-/high-latitudes sites). This applies even more to optical wavelengths, which, in principle, would enable Earth-space communication systems with

extremely high data rates, but, as a matter of fact, are completely obstructed by clouds because of the large density and marked optical extinction properties of micrometric droplets [3].

Significant research efforts have been carried out so far to develop models for the prediction of cloud effects on Earth-space links. Some of them, addressing the EHF range, are mostly of empirical nature; in this class, it is worth mentioning the methodologies conceived by Altshuler and Marr [4] and by Dintelmann and Ortgies [5], which predict cloud attenuation A as a function of some meteorological quantities (e.g. the surface absolute humidity) based on expressions regressed on existing measurements. Other models are more complex as they rely on a simplified cloud model. As an example, the method proposed by Dissanayake *et al.* in [6] estimates cloud attenuation statistics based on four different classes of clouds parameterized using some key average properties (vertical and horizontal extent, water content), as well as their probability of occurrence. The most acknowledged model was developed by Salonen and Uppala (also known as the Teknillinen KorkeaKoulu – TKK – model [7]) and is currently adopted in recommendation ITU-R P.840-6 [8] (henceforth referred to as ‘the ITU-R model’) because of its sound physical basis: the specific attenuation due to suspended liquid water in each atmospheric layer is calculated according to the Rayleigh approximation [9], after identifying clouds from vertical profiles of pressure, relative humidity and temperature (P - RH - T).

Notwithstanding the accuracy of the ITU-R model in predicting cloud attenuation along zenithal links, its drawbacks are, on one side, the assumption that the horizontal distribution of suspended liquid water is uniform (i.e. that clouds attenuation statistics can be scaled from zenithal links to slant paths using the cosecant of the elevation angle) [8] and, on the other side, the fact that the Earth’s curvature is not taken into account. As a matter of fact, these aspects actually prevents the use of the ITU-R model in scenarios involving complex systems distributed in space (e.g. implementing site diversity) [10] or Low Earth Orbit (LEO) satellite applications in which very low elevation links (i.e. long paths through clouds) need to be considered. In addition, the validity of the cloud horizontal homogeneity assumption, and therefore of the cosecant elevation scaling approach, might be questionable even for customary links to geostationary satellite whose θ ranges between 30° and 50° (mid-latitude ground stations).

Manuscript received XXXX.

Lorenzo Luini and Carlo Capsoni are with the Dipartimento di Elettronica, Informazione e Bioingegneria (DEIB), Politecnico di Milano, Piazza Leonardo da Vinci, 35, 20133, Milano, Italy, and with the Istituto di Elettronica e di Ingegneria dell’Informazione e delle Telecomunicazioni (IEIT), Consiglio Nazionale delle Ricerche, Via Ponzio 34/5, Milano 20133, Italy (e-mail: lorenzo.luini@polimi.it).

This contribution investigates the spatial (vertical and horizontal) distribution of clouds by taking advantage of the liquid water content observed by the Cloud Profiling Radar onboard the CloudSat Earth Observation satellite [11]. Besides casting some light on the validity of the above mentioned cloud uniformity assumption, the main goal of this paper is to propose analytical expressions for the scaling factor to derive accurate cloud attenuation statistics on slant paths from attenuation predictions along zenithal links. This, in turn, could improve the accuracy of the ITU-R cloud attenuation model, especially when low elevation links (e.g. between 5° and 20°) are involved. The remainder of this contribution is organized as follows: Section II.A presents the CloudSat data used in this work, while Section II.B and II.C focus on the methodology to scale clouds attenuation statistics with the link elevation. Section II.D gives details on the accuracy of the proposed scaling approach and, finally, Section III draws some conclusions.

II. CLOUD ATTENUATION STATISTICS

A. CloudSat Data

Nowadays, clouds are continuously monitored by means of space-borne scientific equipment onboard Earth Observation satellites. Most of the products derived from remote sensing measurements focus on integral quantities (e.g. total liquid water path) or on specific layers (e.g. cloud top temperature), while few instruments provide information on the whole profile of clouds. The nadir-looking Cloud Profiling Radar (CPR), specifically designed to observe clouds from space, is onboard the NASA CloudSat Earth Observation satellite, which, launched in 2006, flies along a Low Earth Orbit (LEO) as part of the A-Train constellation (Aqua, CloudSat, CALIPSO, PARASOL and Aura satellites). Thanks to its low altitude (around 710 km) and high operational frequency (94 GHz), the CPR measures, with high spatial resolution (the footprint is $1.4 \text{ km} \times 1.7 \text{ km}$ and the vertical profile is sampled every 240 m), the full distribution of the liquid water content $w(h)$ in clouds between the surface and 25 km of altitude [11]. Specifically, we focused on the 2B-CWC-RVOD product developed and distributed by the Cooperative Institute for Research in the Atmosphere (CIIRA) at the Colorado State University [12],[13],[14]. Indeed, these data maximize the accuracy in estimating w because, besides standard calibration and quality checks common to all 2B Level Products, the 2B-CWC-RVOD dataset originates from the combination of CPR-derived profiles and from the concurrent Visible Optical Depth measurements collected by the MODIS sensor that is part of the A-Train constellation as well [12]. Specifically, this joint information is used to estimate the parameters of the particle size distribution (PSD) in each bin containing clouds: radar data provide a vertical profile of the measured cloud backscatter value, while the retrieved visible optical depth values give an estimate of the integrated extinction through the cloud column. For the estimation of w along the vertical profile, the retrieval algorithm assumes that the radius of cloud

droplets follow a lognormal distribution, from which analytical expressions for w and the droplets effective radius r_e can be derived as a function of the main PSD parameters (such as the droplet number density N_T). The retrieval algorithm also takes into account the radar signal attenuation due to the cloud droplets intervening between the radar and the target range bin. Specifically, considering suspended cloud spherical droplets and that their dimension (order of μm) is much smaller than the radar wavelength (order of mm), the Rayleigh approximation of the Mie solution is used to calculate the scattering and absorption properties of cloud particles.

A full year (2009) of CloudSat data covering the whole Globe have been downloaded and processed to study the liquid water content distribution as a function of altitude and of the satellite in-track direction. This is clarified in Fig. 1 Fig. 1 which shows a typical orbit travelled by the CPR aboard CloudSat (top side) and an example of the liquid water content distribution expressed in g/m^3 (bottom side). The latter, depicting heavy equatorial clouds developing up to more than 6 km above that ground, gives a hint of the possible marked spatial variability of the liquid water content, which, in turn, confirms the limited validity of the customary cloud horizontal uniformity assumption [8].

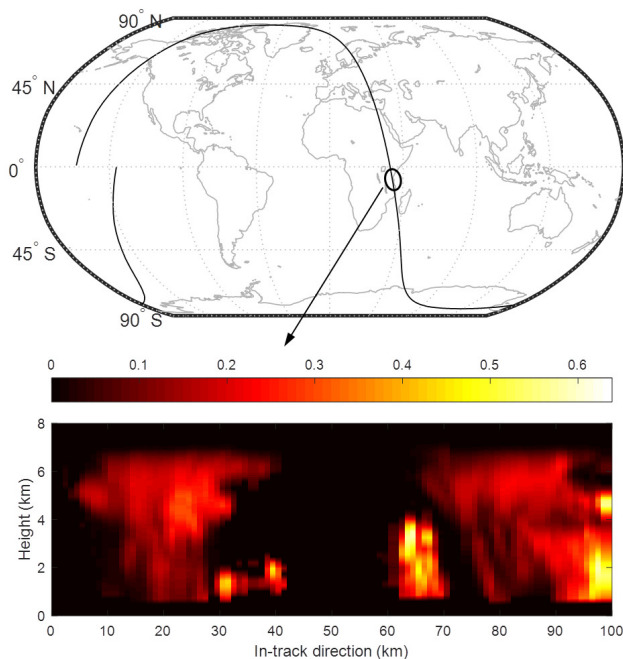


Fig. 1. Typical orbit travelled by the CPR aboard CloudSat (top side) and example of the liquid water content distribution expressed in g/m^3 (bottom side).

B. Calculation procedure

CloudSat data presented in Section II.A offer a unique chance to evaluate the impact of clouds on Earth-space links. Indeed, the knowledge of the full spatial distribution of w as depicted in Fig. 1 Fig. 1 allows identifying the liquid water values impairing a hypothetical electromagnetic link with

elevation angle varying from very low (e.g. $\theta = 5^\circ$) to very high (up to zenithal pointing), which, in turn, allows calculating the liquid water content integrated along the path, L , for every position of the ground station along the CloudSat track. In mathematical terms, L is calculated as:

$$L = \int_P w(l) dl = \sum_{i=1}^N w_i \Delta l \quad (1)$$

where N is the total number of w_i values (i indexing the pixels reported e.g. in Fig. 1) impairing the Earth-space path P and Δl is associated to the pixel dimension.

As a result, it is possible to derive from CloudSat data a clear assessment on the validity of the horizontal uniformity assumption for clouds. This can be achieved by comparing complementary cumulative distribution functions (CCDFs) of L calculated for different elevation angles (to this aim, we have selected $\theta = 5^\circ, 10^\circ, 20^\circ, 30^\circ, 40^\circ, 50^\circ, 60^\circ, 70^\circ$ and 80°) with the one associated to $\theta = 90^\circ$. The final goal is to derive from such a comparison a factor that allows to accurately scale cloud attenuation statistics with the link elevation angle.

Fig. 2 offers an example of shows the yearly CCDFs of L calculated along a zenithal link (L_V , for $\theta = 90^\circ$) and along a slant path (in this example $\theta = 5^\circ$), obtained on one side by using the customary cosecant scaling approach ($L_C = L_V/\sin(\theta)$) and, on the other side, by numerically integrating the liquid water content affecting the slant link (L_S) based on the actual spatial distribution of w (see e.g. Fig. 1). The figure actually reports two curves for L_S , obtained by disregarding (gray dotted line) and by taking into account (gray dashed line) the Earth's curvature (calculation according to section 2.2 of recommendation ITU-R P.676-10 [15], and considering the standard atmospheric profile for which the gradient of the refractive index with height, dn/dh , is assumed to be $-40 \times 10^{-6} \text{ km}^{-1}$ [16]): the divergence between the two curves is not negligible, which points out the need to consider this aspect in cloud attenuation prediction models. For the sake of clarity, all the results presented henceforth will include the effects of the Earth's curvature.

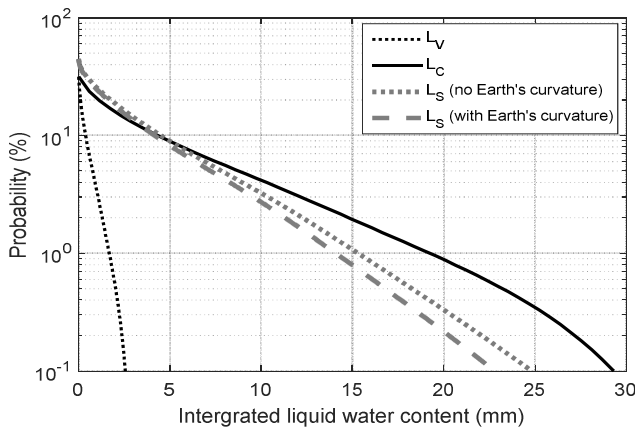


Fig. 2. Sample CCDF of the integrated liquid water content: zenithal link (L_V , for $\theta = 90^\circ$) and slant link ($\theta = 5^\circ$), the latter obtained by using the cosecant scaling approach (L_C) and by numerically integrating the liquid water content

affecting the slant link (L_S) (gray dotted line = no Earth's curvature considered, gray dashed line = effects of Earth's curvature included).

Besides the effects of the Earth's curvature, Fig. 2 also clearly points out the importance of considering the actual spatial distribution of the liquid water content, as the curves associated to L_C and L_S show significant discrepancies: overall, scaling L_V using the customary cosecant law appears to overestimate the actual path liquid water content, while, on the other hand, the probability for clouds to affect the link (i.e. the probability that $L > 0$ mm) is inevitably underestimated by such an approach as clouds might be found along the slant path but not simultaneously above the site where the ground station is located.

All the results included in Fig. 2 are relative to the whole Globe; as a matter of fact, further inspection of the findings suggests the need to separately consider different regions for the calculation of the average CCDFs of L . Indeed in equatorial/tropical areas, convective clouds tend to prevail, while polar regions are mainly covered by stratiform clouds: while the former are typically associated to heavy liquid water content, large vertical extent and marked spatial variability, the latter are usually fairly thin, lie in the lower part of the troposphere and extend quite uniformly in the horizontal direction for many kilometers. After considering several possible latitude belts (and comparing the associated CCDFs of L), the following classification turned out to adequately catch the main climatic differences of interest without introducing unnecessary complexity:

- *Cold zone* (C): latitude $\leq -66^\circ$ N and latitude $\geq 66^\circ$ N
- *Temperate zone* (T): -66° N < latitude $\leq -23^\circ$ N and 23° N \leq latitude < 66° N
- *Equatorial/tropical* (ET) zone: -23° N < latitude < 23° N

As one might expect, cloud statistics are likely to differ from site to site, even if they both pertain to the same climatic zone. Indeed, the latitude belts defined above aim at defining average scaling laws by capturing the main different climatic features across the Globe, while the local diversity of clouds statistics is addressed later on in Section II.D.

Fig. 3 shows the different results obtained for two out of the three zones (to privilege readability the temperate zone has been discarded) by reporting the CCDF of L_S and of L_C for $\theta = 20^\circ$: the probability for liquid water clouds to affect the link is approximately 27%, 40% and 23% for zone C, T and ET, respectively, and, as expected, heavy clouds are more and more likely moving from polar to equatorial regions.

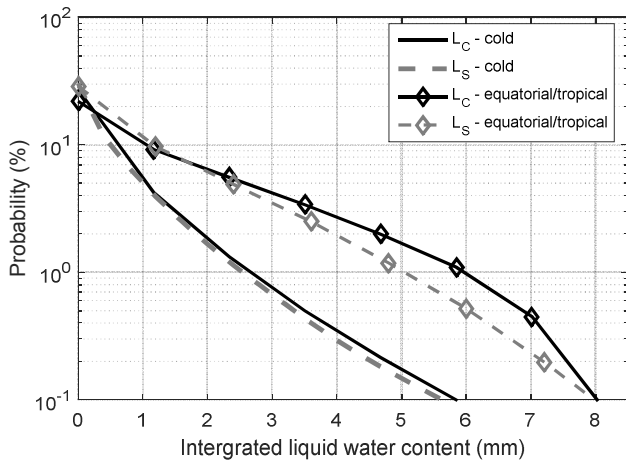


Fig. 3. CCDF of L_S and of L_C for $\theta = 20^\circ$ (cold and equatorial/tropical zones).

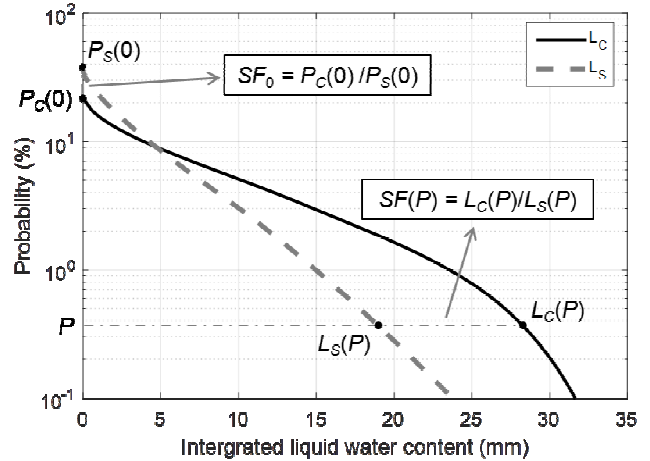


Fig. 4. Definition of the scaling factor based on the CCDF of L_S and of L_C for $\theta = 5^\circ$ (equatorial/tropical zone).

C. Link elevation scaling factor

Besides clearly showing that the climatic zones defined in Section II.B are actually associated to different statistics of L , more importantly, Fig. 3 indicates that, while the horizontal uniformity assumption for clouds basically holds in cold regions even for $\theta = 20^\circ$, this is not the case for the equatorial/tropical zones (as well as for zone T, though not shown in Fig. 3). These discrepancies obviously reflect in the scaling factor, which, as elucidated in Fig. 4, is defined as:

$$SF(P) = L_C(P)/L_S(P) \quad \text{for } L_C > 0 \text{ mm} \quad (2)$$

and

$$SF_0 = P_C(0)/P_S(0) \quad \text{for } L_C = 0 \text{ mm} \quad (3)$$

In (2) and (3), $L_C(P)$ and $L_S(P)$ are the integrated liquid water contents extracted from the cosecant-scaled and slant-path statistics, respectively, both associated to the same probability level P (for any $L_C > 0$ mm), while $P_S(0)$ and $P_C(0)$ are the probability values of the slant-link and cosecant-scaled curves corresponding to $L_C = 0$ mm (probability to have clouds affecting the link). Based on the evaluation of SF and SF_0 calculated for several values of the elevation angle, the expressions in (2) and (3) are valid for $\theta \leq \theta_L$, being $\theta_L = 30^\circ$ for zone C and $\theta_L = 70^\circ$ for zones T and ET, as both scaling factors turn out to be very close to 1 for $\theta > \theta_L$. In fact, as already shown for instance in Fig. 3, the difference between L_C and L_S were found to be negligible (C) or not (ET) depending both on the zone (i.e. on the cloud spatial distribution) and the link elevation angle.

As already pointed out in the discussion above, cloud occurrence might vary significantly from zone to zone and, even more, from site to site; this would render cumbersome the global application of the scaling factor as defined in (1) because the same P level might be associated to intense clouds in a given site and to total absence of clouds in another site. A viable way to solve this issue is to define statistics normalized to the probability to have clouds on the cosecant-scaled link, $P_C(0)$, which corresponds to rigidly shifting upwards both curves in Fig. 4 along the y-axis:

$$\begin{aligned} P_c^* &= P_C / P_C(0) \\ P_s^* &= P_S / P_C(0) \\ P^* &= P / P_C(0) \end{aligned} \quad (4)$$

Fig. 5 shows the scaling factor SF (temperate zone) as a function of the normalized probability level P^* , for three sample elevation angles, namely $\theta = 5^\circ$, 20° and 60° . The following analytical expression is proposed to model SF :

$$SF(P^*) = A(P^*)^B + C \quad \text{for } 10^{-2} \leq P^* \leq P_l \quad (5)$$

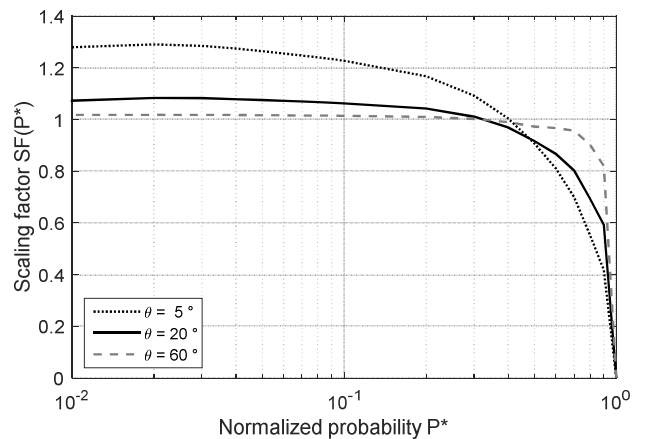


Fig. 5. Scaling factor as a function of the normalized probability level P^* : $\theta = 5^\circ$, 20° and 60° (temperate zone).

> REPLACE THIS LINE WITH YOUR PAPER IDENTIFICATION NUMBER (DOUBLE-CLICK HERE TO EDIT) <

As clarified in (5), the applicability of SF is limited to the range $10^{-2} \leq P^* \leq P_1$. On one side, the lower limit for P^* is set to 10^{-2} because, as already mentioned and as further explained in Section II.D, the diversity in cloud attenuation statistics between sites in the same zone increases more and more as the exceedance probability level decreases (obviously extreme values tend to vary more from site to site) and therefore the applicability of the average SF for $P^* < 10^{-2}$ would yield rather inaccurate results. This is particularly true for the ET zone, characterized by extremely dry areas such as deserts, as well as by sites with heavy precipitations like central Brazil. On the other hand, P_1 , which was found to vary from zone to zone as clarified in Table I, is applied because of the low accuracy of (5) in fitting SF for $P^* > P_1$. As a final remark, it is worth mentioning that, in any case, P_1 must be lower than 1: indeed, for $L_c = 0$ mm ($P^* = 1$ according to (4)), based on (2), $SF = 0$ (i.e. $L_s = L_c / SF \rightarrow \infty$), which prompts to define SF_0 .

TABLE I. VALUE OF P_1 FOR THE THREE ZONES

Region	Cold	Temperate	Equatorial and tropical
P_1	$6.5 \cdot 10^{-1}$	$9.5 \cdot 10^{-1}$	$9.5 \cdot 10^{-1}$

In addition, results pointed out that coefficients A , B and C in (5), plotted as a function of the elevation angle θ , tend to follow quite regular trends, which can be accurately modeled using the following expressions:

$$A = a_A \theta^{b_A} + c_A \quad (6)$$

$$B = a_B \theta^4 + b_B \theta^3 + c_B \theta^2 + d_B \theta + e_B \quad (7)$$

$$C = a_C \theta^{b_C} + c_C \quad (8)$$

Table II lists the values of the coefficients in (6)-(8) for the three zones, while Fig. 6 shows, as an example, the trend of coefficient C with the elevation angle, as well as the fitting expression in (8) (temperate zone).

Similarly to the coefficients in (6)-(8), also the trend of SF_0 with θ can be accurately fitted using the following power-law:

$$SF_0 = D \theta^E + F \quad (9)$$

where D , E and F , different for every zone, are reported in Table III.

TABLE II. SCALING FACTOR COEFFICIENTS FOR PROBABILITY RANGE P_H

Region	Cold	Temperate	Equatorial/tropical
a_A	-1.387	-2.497	-5.85
b_A	-0.8312	-0.1179	-0.0929
c_A	-0.1465	1.027	3.34
a_B	$-2.07 \cdot 10^{-5}$	$1.24 \cdot 10^{-6}$	$1.11 \cdot 10^{-6}$
b_B	0.0014	$-8.48 \cdot 10^{-5}$	$-1.30 \cdot 10^{-4}$
c_B	-0.0309	0.0014	0.0047
d_B	0.2966	0.0643	-0.0258
e_B	0	1.3494	0.9279
a_C	1.48	1.109	2.802
b_C	-1.244	-0.8447	-0.7585
c_C	1.015	0.9739	0.9209

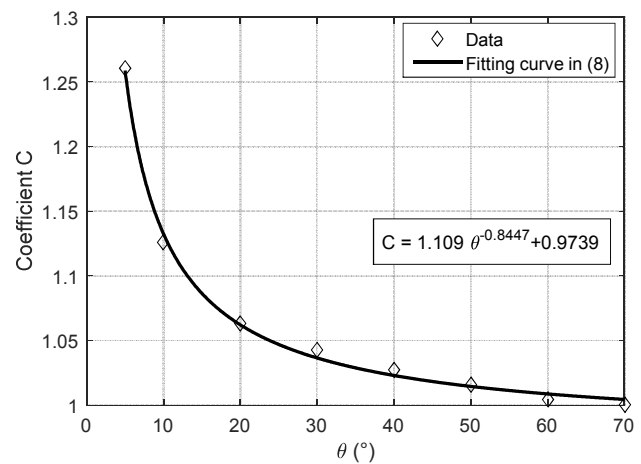


Fig. 6. Trend of coefficient C with the elevation angle, as well as the fitting expression in (8) (temperate zone).

TABLE III. SCALING FACTOR COEFFICIENTS FOR SF_0

Region	Cold	Temperate	Equatorial and tropical
D	0.2581	0.1525	0.3263
E	0.1634	0.2624	0.2223
F	0.4730	0.5139	0.1129

D. Scaling accuracy

This section aims, on one side, at summarizing the full procedure to scale statistics of integrated liquid water content and cloud attenuation with the link elevation using SF and SF_0 and, on the other side, at providing hints on the accuracy of the proposed scaling model when applied to different sites in the same zone.

Since the attenuation due to clouds A is directly proportional to L through the liquid water mass absorption coefficient $a_w(f)$ (see [17] for further details), the scaling factor derived in this work is valid for statistics both of integrated liquid water content and of cloud attenuation, $P(A)$. Thus, according to the proposed method, ~~the~~ $P(A)$ can be scaled with the link elevation following these steps:

1. Start from statistics of A for a zenithal link, $P_V(A_V)$, which can be calculated, for instance, using the ITU-R model in recommendation P.840-6 [8].
2. Obtain the cosecant-scaled curve, $P_C(A_C)$, as: $A_C = A_V/\sin(\theta)$ and $P_C = P_V$.
3. Normalize the cosecant-scaled curve as $P_C^*(A_C) = P_C(A_C)/P_C(0)$ such that $P_C^*(0) = 1$.
4. Sample $P_C^*(A_C)$ with probability levels P^* between P_1 and 10^{-2} , depending on the zone of interest.
5. For every P^* , calculate the normalized slant-path curve, $P_S^*(A_S)$, as: $A_S(P^*) = A_C(P^*)/SF(P^*)$ and $P_S^* = P^*$. $SF(P^*)$ is obtained from equations (6)-(8) and Table II.
6. Calculate the final slant-path statistics, $P_S(A_S)$, as: $P_S(A_S) = P_S^*(A_S) \cdot P_C(0)$.
7. Complete $P_S(A_S)$ by calculating $P_S(0)$ as: $P_S(0) = P_C(0)/SF_0$, where SF_0 is obtained from equations (9) and Table III, depending on the zone of interest.
- 7-8. Finally, A_S values associated to $P_C(0) \cdot P_1 \leq P \leq P_S(0)$, for which SF cannot be applied (see Table I), are obtained by interpolating the curve between the two points defining such range above, i.e. $P_C(0) \cdot P_1$ and $P_S(0)$.

In order to assess the accuracy of the proposed statistics scaling approach, different sites around the Globe have been identified with different climatic features: indeed SF defined by equations (5)-(9) is an average scaling factor because it is derived from all the data included in the three latitude belts, while strong differences might arise among sites in the same zone due to local climatic features (deserts and rain forest). **Fig. 7** depicts the sites selected for the tests (12 circles = ET region, 14 squares = T region, 6 asterisks = C region), for each of which A_V and A_S were calculated using only the CloudSat data included in the $6^\circ \times 6^\circ$ region centered on the site itself. This dimension was found to be a good compromise between preserving the local diversity of clouds while allowing the collection of enough samples to obtain statistically meaningful curves.

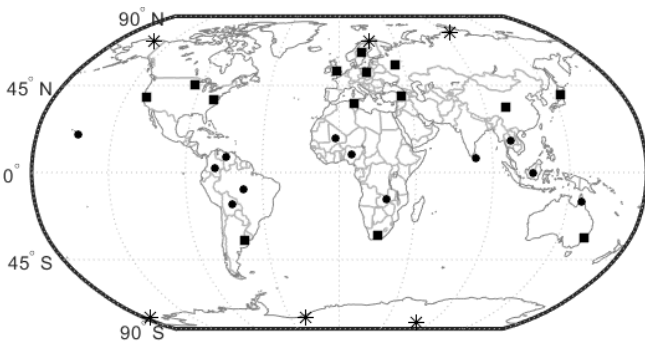


Fig. 7. Sites selected for the tests: 12 circles = ET region, 14 squares = T region, 6 asterisks = C region.

Fig. 8 shows, as an example, the slant-path statistics of A (equatorial/tropical zone, Venezuela, $\theta = 10^\circ$, frequency $f = 30$ GHz, mass absorption coefficient $a_W(f) = 0.8463$ dB/mm calculated based on [17]), as obtained directly through the numerical integration of w derived from CloudSat data (A_S^{ref} in (10)), as well as scaled using the cosecant law or according to ~~the procedure outlined above starting from CloudSat derived statistics of $A_V SF$~~ (A_S^{est} in (10) represents any of the two estimated curves). Results show a close agreement between the two A_S curves, which is quantified in the figure legend using $E\epsilon_A (= 1.1)$ and $RMS\epsilon_A (= 4.4)$, the mean and root mean square values, respectively, of the following error figure (as defined for attenuation statistics in recommendation ITU-R P.311-15 [18][19]):

$$\epsilon_A(P) = \begin{cases} 100 \left[\frac{A_S^{ref}(P)}{10} \right]^{0.2} \ln \left[\frac{A_S^{est}(P)}{A_S^{ref}(P)} \right] & A_S^{ref}(P) < 10 \text{ dB} \\ 100 \ln \left[\frac{A_S^{est}(P)}{A_S^{ref}(P)} \right] & A_S^{ref}(P) \geq 10 \text{ dB} \end{cases} \quad (10)$$

In (10), $A_S^{ref}(P)$ and $A_S^{est}(P)$ are associated to the same probability level $P \geq 5 \times 10^{-1}\%$: in fact, it is worth reminding that, according to (5), the applicability of SF is limited to $P^* \geq 10^{-2}$. On the other hand, the cosecant scaled curve A_C significantly deviates from the reference curve ($E\epsilon_A = 13.5$ and $RMS\epsilon_A = 18.6$).

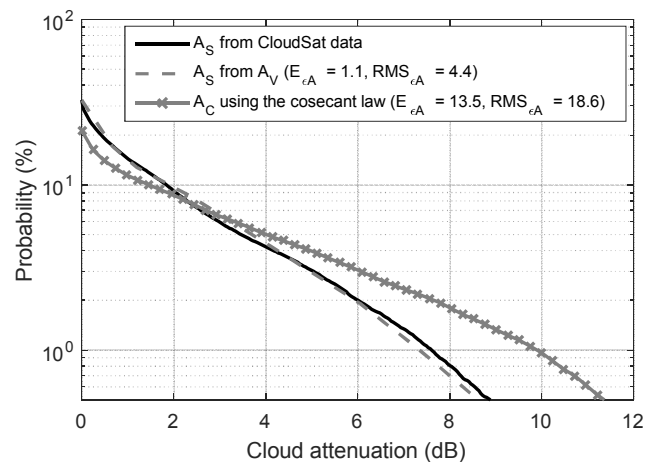


Fig. 8. Accuracy in scaling the CCDF of A in the ET zone (Venezuela) using SF and SF_0 ($\theta = 10^\circ$).

Fig. 9 provides additional information on the accuracy of the proposed scaling approach by showing the overall $E\epsilon_A$ (black dashed lines) and $RMS\epsilon_A$ (gray solid lines) as a function of the link elevation angle for the ET zone (average over all the sites included in the region). Results obtained using the scaling based on SF and SF_0 (lines with circles) and

based on the cosecant law (lines with squares) are compared. The former methodology shows only a slight decrease in the accuracy for $\theta = 5^\circ$ and 10° , while the scaling error increases drastically for the cosecant law when θ gets smaller. Moreover, while the proposed approach is rather unbiased ($E_{\mathcal{E}_A}$ close to 0), the cosecant law, as expected, yields a marked overestimation.

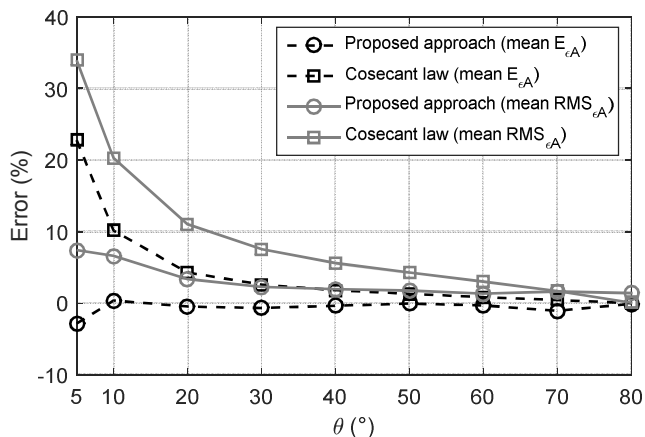


Fig. 9. Overall accuracy in scaling the CCDF of A as a function of the link elevation angle (average overall all the sites in the region).

As additional information, Fig. 10 depicts the overall prediction error as a function of the different sites spanning the whole T region: for both approaches, results indicate quite a stable prediction performance, notwithstanding the robust climatic differences existing, for instance, between North Africa (site 4) and Sweden (site 11). Further investigations on all the three regions (overall error as a function of the link elevation in the C zone) show results similar to those reported in Fig. 9 and Fig. 10.

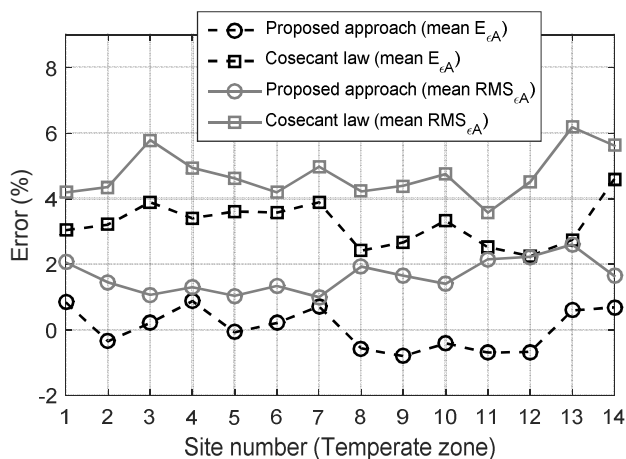


Fig. 10. Overall accuracy in scaling the CCDF of A for different sites in the T region (average overall all the link elevation values).

III. CONCLUSIONS

This contribution presents a methodology to accurately scale cloud attenuation statistics with link elevation θ in Earth-space applications, based on vertical profiles of the liquid

water content collected by the Cloud Profiling Radar onboard the CloudSat LEO satellite.

The extensive dataset, first processed to calculate statistics of integrated liquid water content for values of θ between 5° and 90° , indicates the importance of taking in due account the effects introduced on an hypothetical link by the Earth's curvature and, moreover, that the horizontal uniformity assumption for clouds, i.e. the customary cosecant scaling approach typically adopted e.g. in the cloud attenuation prediction model currently recommended by ITU-R in P.840-6, is valid for link elevations higher than 30° and 70° for cold (polar) zones (latitude $\leq -66^\circ$ N and latitude $\geq 66^\circ$ N) and for the rest of the Globe, respectively. These findings are expected as they reflect the different spatial distribution of clouds moving across latitudes, which, in turn, is linked to the prevalence of stratiform and convective clouds in cold and equatorial/tropical zones, respectively.

The scaling factor SF is derived from the statistics of L at different elevation angles and analytical expressions for SF are proposed to derive accurate cloud attenuation statistics on slant paths from attenuation predictions along zenithal links. Such expressions, separately provided for cold, temperate and equatorial/tropical zones as simple function of the link elevation, are tested in different sites across the Globe: results indicate a fairly stable prediction performance, notwithstanding the robust climatic differences that might exist among sites within the same zone. The scaling approach proposed in this contribution could be beneficial to improve the accuracy of the ITU-R cloud attenuation model, especially when low elevation links (e.g. between 5° and 20°) are involved.

ACKNOWLEDGMENT

The authors would also like to acknowledge the CloudSat mission scientists and associated NASA personnel for the production of the data used in this work.

REFERENCES

- [1] R. K. Crane, "Electromagnetic Wave Propagation Through Rain," Wiley, 1996.
- [2] C. Capsoni, L. Luini, A. Paraboni, C. Riva, A. Martellucci, "A new prediction model of rain attenuation that separately accounts for stratiform and convective rain," *IEEE Transactions on Antennas and Propagation*, Vol 57, No. 1, January 2009, Page(s): 196 - 204.
- [3] L. Luini, R. Nebuloni, C. Capsoni, "Effectiveness of Multisite Diversity Schemes to Support Optical Systems in Scientific Missions," *Optical Engineering*, 53 (2), 026104 (Feb 18, 2014).
- [4] E. Altshuler, R. Marr, "Cloud attenuation at millimetre wavelengths," *IEEE Transactions On Antennas and Propagation*, 37, 1473-1479, 1989.
- [5] F. Dintelmann, G. Orgies, "Semi-empirical model for cloud attenuation prediction," *Electron. Lett.*, 25, 1487-1479, 1989.
- [6] A. Dissanayake, J. Allnut, F. Haidara, "Cloud attenuation modelling for SHF and EHF applications," *Int. J. Satell. Commun.* 2001; 19:335-345.
- [7] E. Salonen, S. Uppala, "New prediction method of cloud attenuation," *Electron. Lett.*, vol. 27, no. 12, pp. 1106-1108, Jun. 1991.
- [8] Attenuation due to clouds and fog. Geneva, 2013, ITU-R recommendation P.840-6.

> REPLACE THIS LINE WITH YOUR PAPER IDENTIFICATION NUMBER (DOUBLE-CLICK HERE TO EDIT) <

8

- [9] H. J. Liebe, "MPM - An atmospheric millimeter-wave propagation model," *Int. J. Infrared and Millimeter Waves*, 1989, 10, pp. 631450.
- [10] L. Luini, C. Capsoni, "A Rain Cell Model for the Simulation and Performance Evaluation of Site Diversity Schemes," *IEEE Antennas and Wireless Propagation Letters*, Vol. 12, No. 1, Page(s): 1327-1330, 2013.
- [11] G. L. Stephens, D. G. Vane, R. J. Boain, G. G. Mace, K. Sassen, Z. Wang, A. J. Illingworth, E. J. O'Connor, W. B. Rossow, S. L. Durden, S. D. Miller, R. T. Austin, A. Benedetti, C. Mitrescu, the CloudSat Science Team, "The CloudSat mission and the A-TRAIN: A new dimension to space-based observations of clouds and precipitation," 2002, *Bull. Am. Met. Soc.*, 83, 1771-1790.
- [12] N. Wood, "Level 2B Radar-Visible Optical Depth Cloud Water Content (2B-CWC-RVOD) Process Description Document," CloudSat project, Version 5.1, 23 October 2008; available online at http://www.cloudsat.cira.colostate.edu/ICD/2B-CWC-RVOD/2B-CWC-RVOD_PDD_V5p1.pdf.
- [13] Y. Hong, G. Liu, "The Characteristics of Ice Cloud Properties Derived from CloudSat and CALIPSO Measurements," *Journal of Climate* 28(9):150226133621007, February 2015.
- [14] L. Wang, C. Li, Z. Yao, "Application of aircraft observations over Beijing in cloud microphysical property retrievals from CloudSat," *Advances in Atmospheric Sciences* 31(4), July 2014.
- [15] ITU-R Recommendation P.676-10, Attenuation by atmospheric gases. Geneva, Switzerland, 2013.
- [16] ITU-R Recommendation P.452-16, Prediction procedure for the evaluation of interference between stations on the surface of the Earth at frequencies above about 0.1 GHz. Geneva, Switzerland, 2015.
- [17] L. Luini, C. Capsoni, "Efficient Calculation of Cloud Attenuation for Earth-space Applications," *IEEE Antennas and Wireless Propagation Letters*, vol. 13, Page(s): 1136 - 1139, 2014.
- [18] ITU-R Recommendation P.311-15, Acquisition, presentation and analysis of data in studies of tropospheric propagation. Geneva, Switzerland, 2015.